LUNG CELLULAR AND MOLECULAR PHYSIOLOGY.

Am J Physiol Lung Cell Mol Physiol 327: L557–L573, 2024. First published August 27, 2024; doi:10.1152/ajplung.00149.2023

RESEARCH ARTICLE

Developing a mouse model of human coronavirus NL63 infection: comparison with rhinovirus-A1B and effects of prior rhinovirus infection

J. Kelley Bentley,¹ Jordan E. Kreger,¹ Haley A. Breckenridge,¹ Shilpi Singh,¹ Jing Lei,¹ Yiran Li,¹ Susan C. Baker,³ © Carey N. Lumeng,^{1,2} and © Marc B. Hershenson^{1,2}

¹Department of Pediatrics, University of Michigan Medical School, Ann Arbor, Michigan, United States; ²Department Molecular and Integrative Physiology, University of Michigan Medical School, Ann Arbor, Michigan, United States; and ³Department of Microbiology and Immunology, Loyola University Chicago Stritch School of Medicine, Maywood, Illinois, United States

Abstract

Human coronavirus (HCoV)-NL63 causes respiratory tract infections in humans and uses angiotensin-converting enzyme 2 (ACE2) as a receptor. We sought to establish a mouse model of HCoV-NL63 and determine whether prior rhinovirus (RV)-A1B infection affected HCoV-NL63 replication. HCoV-NL63 was propagated in LLC-MK2 cells expressing human ACE2. RV-A1B was grown in HeLa-H1 cells. C57BL6/J or transgenic mice expressing human ACE2 were infected intranasally with sham LLC-MK2 cell supernatant or 1×10^5 tissue culture infectious dose (TCID₅₀) units HCoV-NL63. Wild-type mice were infected with 1×10^6 plaque-forming units (PFU) RV-A1B. Lungs were assessed for vRNA, bronchoalveolar lavage (BAL) cells, histology, HCoV-NL63 nonstructural protein 3 (nsp3), and host gene expression by next-generation sequencing and qPCR. To evaluate sequential infections, mice were infected with RV-A1B followed by HCoV-NL63 infection 4 days later. We report that hACE2 mice infected with HCoV-NL63 showed evidence of replicative infection with increased levels of vRNA, BAL neutrophils and lymphocytes, peribronchial and perivascular infiltrates, and expression of nsp3. Viral replication peaked 3 days after infection and inflammation persisted 6 days after infection. HCoV-NL63-infected hACE2 mice showed increased mRNA expression of IFNs, IFN-stimulated proteins, and proinflammatory cytokines. Infection with RV-A1B 4 days before HCoV-NL63 significantly decreased both HCoV-NL63 vRNA levels and airway inflammation. Mice infected with RV-A1B prior to HCoV-NL63 showed increased expression of antiviral proteins compared with sham-treated mice. In conclusion, we established a mouse model of HCoV-NL63 replicative infection characterized by relatively persistent viral replication and inflammation. Prior infection with RV-A1B reduced HCoV-NL63 replication and airway inflammation, indicative of viral interference.

NEW & NOTEWORTHY We describe a mouse model of human coronavirus (HCoV) infection. Infection of transgenic mice expressing human angiotensin-converting enzyme 2 (ACE2) with HCoV-NL63 produced a replicative infection with peribronchial inflammation and nonstructural protein 3 expression. Mice infected with RV-A1B 4 days before HCoV-NL63 showed decreased HCoV-NL63 replication and airway inflammation and increased expression of antiviral proteins compared with sham-treated mice. This research may shed light on human coronavirus infections, viral interference, and viral-induced asthma exacerbations.

asthma; coronavirus; rhinovirus; interference; interferon

INTRODUCTION

The human coronaviruses (HCoV) 229E and OC43 were first isolated from patients with respiratory illness in the 1960s (1–3). Volunteers inoculated with HCoV-229E and HCoV-OC43 developed a common cold (4). HCoV-NL63 was first isolated from a 7-mo-old patient with bronchiolitis and conjunctivitis in the Netherlands in 2003, and HCoV-HKU1 was isolated from a 71-yr-old patient with pneumonia in Hong Kong in 2004 (5, 6). These human coronaviruses are generally not life-threatening in healthy individuals, causing the common colds and croup in children and young adults. However, outbreaks of highly pathogenic human coronaviruses, severe acute respiratory syndrome (SARS)-CoV, Middle

East respiratory syndrome (MERS)-CoV, and SARS-CoV-2, emerged in 2002 (7), 2012 (8) and 2019 (9).

The family Coronaviridae comprises a large group of viruses with broad host tropism and is divided into two subfamilies and five genera. HCoV-229E and HCoV-NL63 are grouped into the genus *Alphacoronavirus*, and HCoV-OC43, HCoV-HKU1, MERS-CoV, SARS-CoV, and SARS-CoV-2 into *Betacoronavirus* (10). Coronaviruses are enveloped positive-stranded RNA viruses with extended spike proteins on the surface. The envelope consists of a lipid bilayer in which the membrane (M), envelope (E), and spike (S) structural proteins are anchored. Inside the envelope is the nucleocapsid, which is formed from multiple copies of the nucleocapsid (N) protein bound to the positive-sense single-stranded RNA

Check for updates

genome. Coronavirus genome size ranges from 26 to 32 kB, one of the largest among RNA viruses. The genome carries a 5' methylated cap and a 3' polyadenylated tail and harbors two large open reading frames (11, 12). ORF1a and ORF1b encode the 16 nonstructural proteins indispensable for viral replication [nonstructural protein (nsp)1-16]. Later ORFs encode the four structural proteins and multiple accessory proteins.

Coronavirus-19 (COVID-19) disease, caused by SARS-CoV-2, is now a leading cause of death in the United States. Although HCoV-NL63 is not considered life-threatening in healthy individuals, HCoV-NL63 carries some similarities to SARS-CoV-2. Like SARS-CoV and SARS-CoV-2, the HCoV-NL63 spike (S) uses angiotensin-converting enzyme 2 (ACE2) as a receptor albeit the NL63 spike has been shown to bind with less affinity (13). Furthermore, in immunocompromised patients, HCoV-NL63 may cause similar clinical syndromes as SARS-CoV-2. Infection with coronavirus may be more serious in immunocompromised or elderly adults (14–16). In a study of patients with acute respiratory disease warranting presentation to Queensland, Australia hospitals, HCoV-NL63 positive individuals often showed abnormal chest radiographs (56%), respiratory distress (50%), wheeze (44%), and rales (25%) (17). COVID-19 can spread rapidly in long-term residential care facilities (18). In an outbreak of HCoV-NL63 in a long-term care facility in Louisiana, 6 of 20 patients were hospitalized with pneumonia and 3 died (19). Finally, like SARS-CoV-2 (20), an association between HCoV-NL63 and systemic inflammation in children has been described (21). Since studies of SARS-CoV-2 require BSL-3 containment, we wanted to develop a system to study human CoVs using an informative BSL-2 animal model system.

We sought to establish a mouse model of HCoV-NL63 by infecting transgenic mice expressing human ACE2. These mice have been used to study SARS-CoV and SARS-CoV-2 infection in vivo (22, 23). We hypothesize that expression of human ACE2 in mice permits HCoV-NL63 infection.

We previously developed a mouse model of rhinovirus (RV)-A1B infection, a minor group virus which binds to the low-density lipoprotein receptor (LDL-R). Based on partial homology between human and mouse LDL-R, mice infected with RV-A1B show limited viral replication, as evidenced by interferon (IFN) production and the presence of doublestranded viral RNA (24). We compared the effects of RV-A1B and HCoV-NL63 on lung inflammation and gene expression.

Finally, RV infection blocks SARS-CoV-2 replication in cultured airway epithelial cells (25) and airway epithelial organoids (26). We therefore tested whether RV-A1B infection blocks HCoV-NL63 infection in our in vivo model.

MATERIALS AND METHODS

Antibodies to HCoV-NL63 Proteins

Rabbit polyclonal antibodies against HCoV-NL63 the nsp3 peptide sequence YIYDEEGGYDVSKPV and the nucleoprotein sequence DKPSQLKKPRWKRVP were generated by GenScript (Piscataway, NJ). Carboxy terminal cysteines were added to allow conjugation to hemocyanin. Purified primary antibodies were labeled for immunofluorescence using AlexaFluor dye-conjugated N-hydroxy succinimidyl esters, as described (27).

Viral Preparation

HCoV-NL63 and LLC-MK2 cells were obtained from BEI Resources (Manassas, VA). LLC-MK2 cells permissive for HCoV-NL63 infection (28, 29) were transformed with the human ACE2 lentiviral vector pLV[Exp]-mCherry:T2A:Puro-CMV > hACE2[NM_021804.3] (VectorBuilder, Chicago, IL) and selected with puromycin (0.5 µg/mL). Lentivirus-infected cells stably expressing human ACE2 were easier to grow and maintain several days postinfection than the original LLC-MK2 cell line. Infection was confirmed by staining with anti-HCoV-NL63 nucleoprotein (Fig. 1A). Infected LLC-MK2-ACE2 cells were harvested by scraping the plates, lysed with a sterile ground glass homogenizer, and centrifuged at 10,000 g. Cell supernatants were used for infections. The viral cytopathic effect in LLC-MK2-ACE2 cells at 72 h postinfection was measured to determine the tissue culture infectious dose (TCID₅₀) by the Spearman–Karber method (30). HCoV-NL63 infection was confirmed by staining with anti-HCoV-NL63 nucleoprotein (Fig. 1A). Fresh LLC-MK2-ACE2 supernatants usually held a TCID₅₀ of $\sim 1 \times 10^7$ /mL. Primers from the HCoV-NL63 sequence (NC_005831.2) were used to measure viral copy number (vRNA) by qPCR (Table 1). A plasmid containing bases 1–540 of the sequence was used as a copy number standard (GenScript).

RV-A1B viral stocks (ATCC, Manassas, VA) were grown in HeLa-H1 cells, concentrated, and partially purified by ultrafiltration with a 100 kD filter (viral particles do not pass through the filter), and titered by plaque assay as previously described (31, 32).

To evaluate for cross contamination of viral stocks, RNA samples from RV-A1B-infected HeLa-H1 cells and HCoV-NL63-infected LLC-MK2-ACE2 cells were analyzed by nextgeneration sequencing. Total RNA was prepared using Trizol extraction (InVitrogen, Carlsbad, CA) and purified using RNEasy spin columns (Qiagen, Germantown, MD). After on column DNAse I digestion (Qiagen), samples were submitted for ribosomal RNA depletion, library production, and RNA sequence analysis to Azenta Life Sciences (Burlington, MA). The RV-A1B sample had 2749837 hits for the NC_ 038311.1 genome corresponding to RV-A1B and no hits for NC_005831.2 genome corresponding to HCoV-NL63. The HCoV-NL63 sample had 107 hits for the NC_038311.1 (RV-A1) genome and 627,140 hits for the NC_005831.2 (NL63) genome.

Infection of Wild-Type C57BL/6 and Human ACE2 **Transgenic Mice**

All animal research was performed according to the Guide for the Care and Use of Laboratory Animals (8th ed., National Academies Press, 2011) and the American Veterinary Medical Association Guidelines for the Euthanasia of Animals. The protocols were approved by the University of Michigan Animal Care and Use Committee (Protocol No. PRO00010065). All mouse treatments were administered under isoflurane anesthesia. Experimental animals were humanely euthanized at defined end points by exposure to isoflurane vapors followed by thoracotomy.

Table 1. Oligonucleotide primers used for qPCR

	Sequence
Human ACE2 genomic (forward)	5'-GGA TGG AGT ACC GAC TGG AG-3'
	5'-CAT ATG CTT TAT CTC CAA GAG CTG-3'
	5'-/56-FAM/ AGA CCA AAG CAT CAA AGT GAGG/3BHQ 1/-3'
	5'-AGA AAG CAG TCT GCC ATC CC-3'
	5'-GCT GTC AGG AAG TCG TCC AT-3'
	5'-CAC GTG GGC TCC AGC ATT-3'
	5'-TCA CCA GTC ATT TCT GCC TTT G-3'
	5'-/5Cy5/ CCA ATG GTC GGG CAC TGC TCAA/3BHQ 2/-3'
	5'-GAT AGA GAA TTT TCT TAT TTA GAC TTT GT-3'
	5'-TGC CAT AAC AAA TGA CAG CAC T-3'
	5'-GTC CTC CGG CCC CTG AAT G-3'
	5'-GAA ACA CGG ACA CCC AAA GTA G-3'
	5'-CCA TCC CTG TCC TGA GTG-3'
	5'-CCA TGC AGC AGA TGA GTC CTT-3'
	5'-TGG CTG TTT CTG GCT GTT AC-3'
3 ()	5'-TCC ACA TCT ATG CCA CTT GAG TT-3'
	5'-TGC ACC CAA ACC GAA GAA GTC AT-3'
	5'-CAA GGG AGC TTC AGG GTC AAG-3'
	5'-GCT GCA ACT GCA TCC ATA TC-3'
	5'-TTT CAT CGT GGC AAT GAT CT-3'
	5'-CAG CCC TCT CCATCA ACT ATA AG-3'
	5'-CCT GTA GGT GAG GTT GAT CTT TC-3'
	5'-CTT GAG AAG GAC ATG AGG TGC AG-3'
,	5'-GGT CAG GGC TGA GTC ATT TAT GTT-3'
	5'-CCG GAG CCA AGA TCC CAT T-3'
	5'-TGC CTG CCC TGC TTA GTT TG-3'
	5'-AAG CGC CTG CTA CAC AAG AAC-3'
	5'-TAG AGC TCC ATT GTG GCC CTG-3'
9 ()	5'-GAC ATA GTG GCT CAG CGG G-3'
	5'-ATA TCG GGT GCT CTC TTC ACC-3'
	5'-GCA GTC ATC AGA GTG CAA GC-3'
	5'-TCA CCA GAA AGG ACA TCC TCG-3'
Mouse Mx2 (forward)	5'-ACC AGG CTC CGA AAA GAG TT-3'
	5'-TCT CGT CCA CGG TAC TGC TT-3'
	5'-GTC GGT GTG AAC GGA TTT G-3'
	5'-GTC GTT GAT GGC AAC AAT CTC-3'
Mouse NIrp3 (forward)	5'-TGC TCT TCA CTG CTA TCA AGC CCT-3'
Mouse Nirp3 (reverse)	5'-ACA AGC CTT TGC TCC AGA CCC TAT-3'
	5'-TCG TTC ATC TCT GGA GCA TC-3'
Mouse <i>Tlr2</i> (reverse)	5'-TTG ACG CTT TGT CTG AGG TT-3'
Mouse II1b (forward)	5'-TGG CAG CTA CCT GTG TCT TTC-3'
Mouse II1b (reverse)	5'-GGA TGG GCT CTT CTT CAA AGA TG-3'
Mouse Cxc/2 (forward)	5'-GCG CTG TCA ATG CCT GAA G-3'
Mouse Cxc/2 (reverse)	5'-CGT CAC ACT CAA GCT CTG GAT-3
	5'-CTG TTC TGC ACA AAG GAT GGG-3'
Mouse II1f6 (reverse)	5'-AGA GAG AGG CTT TTA CAG GTT C-3'
	5'-GCC TGA GAG CTG CCC CTT CAC-3'
	5'-GGC TGC CTG GCG GAC AAT CG-3'
	5'-CTC CTG GTT TGC CAT CGT TT-3'
	5'-GGG AGT CCA GTC CAC CTC TA-3'
Mouse II21 (forward)	5'-TCC ACA AGA TGT AAA GGG GCA-3'
	5'-TGA TGG CTT GAG TTT GGC CT-3'

5Cy5, 5' cyanine 5; 3BHQ, black hole quencher, 1 for FAM, 2 for Cy5; 56-FAM. 5' 6-carboxyfluorescein.

B6.Cg-Tg(K18-ACE2)2Prlmn/J mice (Jackson Laboratories, Bar Harbor, ME) express the human ACE2 protein in epithelial cells using the keratin 18 promoter (22). Mice were genotyped using the vendor-recommended protocol and confirmed by measurement of human ACE2 mRNA expression by qPCR (primers are listed in Table 1). Eight-to-tenweek-old male and female K18-hACE2 or C57BL6/J mice were inoculated with 50 μ L of 1 \times 10⁵ TCID₅₀ HCoV-NL63 or sham LLC-MK2-ACE2 supernatant intranasally and euthanized at 1–7 days posttreatment. The 10,000 g supernatant fluid of homogenized, uninfected LLC-MK2-ACE2 cells was used for sham infections.

Selected K18-hACE2 or C57BL6/J mice were infected intranasally with 50 μL RV-A1B [1 \times 10⁶ plaque-forming units (PFU)] (24). In some experiments, mice were infected with RV-A1B or LLC-MK2-ACE2 supernatant 4 days prior to HCoV-NL63 infection.

Histology, Immunofluorescence, and Immunoblotting

After euthanasia, mouse right arteries were perfused with PBS + 5 mM EDTA. The tracheas were intubated, and the lungs were inflated with formalin and processed for paraffin sectioning. Sections were stained with hematoxylin and eosin or immunofluorescence imaging for anti-HCoV nucleoprotein, anti-nsp3 (GenScript), and anti-double-stranded (ds)RNA (clone rJ2, Sigma-Aldrich, Burlington, MA). Lung lysates were also analyzed for nsp3 protein expression and β-actin by immunoblotting. Lungs were homogenized in lysis buffer containing 1% triton X-100 and protease inhibitors (Sigma-Aldrich). Insoluble particles were removed by centrifugation for 30 min at 4°C, and total protein was measured by bicinchoninic acid (BCA) assay (ThermoFisher, Waltham, MA). Cell extracts were resolved by 10% SDS-PAGE, and proteins were transferred to a nitrocellulose membrane. Membranes were blocked with 5% low-fat dry milk in Tris-buffered saline with 0.05% Tween-20 (Sigma-Aldrich). For nsp3 immunoblotting, lanes were loaded with 50 µg of total protein, and membranes were probed with 0.1 µg/mL anti-nsp3 (GenScript). Signals were amplified and visualized with 0.01 $\mu g/mL$ goat anti-rabbit IgG-horseradish peroxidase conjugate (ThermoFisher) and chemiluminescence solution (Pierce, Rockford, IL). For β-actin immunoblotting, lanes were loaded with 20 μg of total protein, membranes were probed with 0.01 µg/mL mouse monoclonal anti- β -actin (Sigma-Aldrich), and amplified with 0.01 µg/mL rat anti-mouse IgG kappa chain-horseradish peroxidase conjugate (ThermoFisher).

Bronchoalveolar Lavage

Mouse lungs were processed for bronchoalveolar lavage (BAL) using 1 mL PBS aliquots (33). Cytospins were stained with hematoxylin and eosin (Sigma-Aldrich), and differential counts were determined from 200 cells.

Next-Generation RNA Sequencing

RNA library generation and next-generation sequencing were performed by the University of Michigan Advanced Genomic Core. Total RNA was prepared using Trizol extraction (Invitrogen). RNA was double purified using RNEasy spin columns (Qiagen) and enriched for mRNA using a Poly (A) mRNA Magnetic Isolation Module (New England Biolabs, Ipswich, MA). cDNA libraries for next-generation sequencing were prepared with a xGen Broad-Range RNA Library Prep (IDT, Coralville, IA) with xGen Normalase UDI Primers (IDT). Samples were subjected to 151 bp paired-end sequencing using a NovaSeq S4 flow cell (Illumina, SanDiego, CA) according to the Illumina NovaSeg manufacturer's protocol. Reads were mapped to the reference genome GRCm38 (ENSEMBL 102) using STAR v2/7.8a (34) and assigned count estimates to genes with RSEM v1/3.3(35).

Quantitative Polymerase Chain Reaction

Total RNA was prepared using Trizol extraction and RNAeasy purification (Qiagen). First-strand cDNA was prepared using the SuperScript IV system (Applied Biosystems, Waltham, MA). Transcript abundance relative to GAPDH was estimated by quantitative polymerase chain reaction (qPCR) using primers listed in Table 1. Viral copy number was measured as described earlier.

Enzyme-Linked Immunosorbent Assay

Selected cytokines were measured in the bronchoalveolar lavage fluid by enzyme-linked immunosorbent assay (ELISA). We measured levels of IL-36α (MyBioSource, San Diego, CA), IL-1β (Invitrogen, Waltham, MA), IFN-α1 (BioLegend, San Diego, CA), and IFN-λ2/3 (R&D Systems, Minneapolis, MN). In addition, CXCL1, CXCL2, and CXCL5 cytokine concentrations were measured by the University of Michigan Cancer Center Immunology Core using DuoSet ELISA kits (R&D Systems).

Measurement of Airways Responsiveness

Mice were anesthetized, intubated, and ventilated with a Buxco FinePointe System (Data Sciences International, St. Paul, MN). Methacholine was administered by nebulizer as previously described (33).

Data Analysis

For most experiments, statistical significance was assessed by the Kruskal-Wallis test for nonparametric data. Group differences were pinpointed by the Dunn's multiple comparisons test. For airways resistance data, statistical significance was assessed by two-way analysis of variance. Group differences were pinpointed by the two-stage linear step-up procedure of Benjamini, Krieger, and Yekutieli. A P value less than 0.05 was considered statistically significant. Adjusted P values were rounded according to the American Physiological Society guideline (36). All data are represented in box and whisker plots, showing the median, 25th and 75th percentiles (the hinges of the box), and min and max (location of the

For RNA sequencing (RNA-Seq) analysis, gene expression was estimated according to the expected count totals

Table 2. List of GO groups examined for fold change 1.5 after infection with HCoV-NI 63 and RV-A1R

>1.5 after infection with HCoV-NL63 and RV-A1B	
Process	
1 GO:0001775	Cell activation
2 GO:0001776	Leukocyte homeostasis
3 GO:0001816	Cytokine production
4 GO:0002200	Somatic diversification of immune receptors
5 GO:0002252	Immune effector process
6 GO:0002253	Activation of immune response
7 GO:0002262	Myeloid cell homeostasis
8 GO:0002339	B cell selection
9 GO:0002404	Antigen sampling in mucosal-associated lymphoid tissue
10 GO:0002440	Production of molecular mediator of immune response
11 GO:0002507	Tolerance induction
12 GO:0002520	Immune system development
13 GO:0002532	Production of molecular mediator involved in
	inflammatory response
14 GO:0002682	Regulation of immune system process
15 GO:0002683	Negative regulation of immune system process
16 GO:0002684	Positive regulation of immune system process
17 GO:0006955	Immune response
18 GO:0007017	Microtubule-based process
19 GO:0007267	Cell-cell signaling
20 GO:0019882	Antigen processing and presentation
21 GO:0023056	Positive regulation of signaling
22 GO:0023057	Negative regulation of signaling
23 GO:0031294	Lymphocyte costimulation
24 GO:0045058	T cell selection
25 GO:0045321	Leukocyte activation
26 GO:0050900	Leukocyte migration
27 GO:0090713	Immunological memory process

GO, gene ontology; HCoV, human coronavirus; RV, rhinovirus.

extracted through sequence alignment. Differential gene expression for HCoV-NL63 versus sham and RVA-1B versus sham was determined using R package DESeq2 v1/38.1 with default parameters (37). DESeq2 uses an empirical Bayes approach to integrate the dispersion and fold change estimates and tests the gene differential expression using the Wald test. The Wald test *P* values were adjusted for multiple testing using the procedure of Benjamini and Hochberg. Genes with an adjusted P value less than 0.05 were considered statistically significant. Of note, sequencing of specimens collected 4 days after viral infection was performed at a later date than sequencing of day 2 specimens, allowing the possibility of batch effects. Potential batch effects were considered to be negligible. Also, because of the small number of samples, we also noted genes as those with a fold change of >1.5 or <0.66 (log 2 fold change >0.585 or \leq -0.585). Using the R package clusterProfiler v4/6.0 (38), differentially expressed genes were categorized into biological process gene ontology groups at level 3 specificity. We focused on 27 gene ontology groups related to the immune process (see Table 2). Individual upregulated genes of interest—for example, genes encoding interferons (IFNs), interferon-stimulated genes, and proinflammatory cytokines and chemokines—were selected for fold change comparison.

RESULTS

HCoV-NL63 Propagation in K18-hACE2 Mice

Adult K18-hACE2 and C57BL6/J mice were infected with 1×10^5 TCID₅₀ HCoV-NL63 or sham intranasally and euthanized at 0-6 days posttreatment. Viral copy number was assessed by qPCR and conventional PCR (Fig. 1B). The amount of "input" virus was measured 2 h after inoculation and did not differ between mouse strains. Because mice are relatively nonpermissive to human viral infections, viral copy number fell precipitously after inoculation of both C57BL6/J and hACE2 strains. Viral copy number appeared to increase with time in both strains, but median lung vRNA rose above the input amount only in the hACE2 mice (3 and 4 days after inoculation). Also, only samples from hACE2 mice showed a clear HCoV-NL63 PCR band 1-5 days after infection. The only solid band for the C57BL/6 mice occurred 2 h after inoculation, representing the viral input. Later time points for the C57BL/6 mice showed nonspecific bands, which may have led to an elevation of the qPCR signal. Immunoblots of the HCoV-NL63 nonstructural protein nsp3 showed a similar pattern (Fig. 1C), with a strong band 2 and 4 days after inoculation only in hACE2 mice. HCoV-NL63 nucleoprotein was detected on the apical surface of airway epithelial cells of HCoV-NL63-infected K18-hACE2 mice but not sham-infected K18-hACE2 mice, and Nsp3 was detected in the cytoplasm of airway epithelial cells (Fig. 1D). Induction of lung IFNα1 mRNA expression (Fig. 1E) was significantly higher in hACE2 mice than C57BL/6 mice, further evidence of viral replication (39). Together, these data demonstrate that meaningful viral replication occurred in HCoV-NL63-infected hACE2 mice but was negligible in C57BL/6 mice.

HCoV-NL63 Infection Induces Airway Inflammation in hACE2 Mice

HCoV-NL63 infection did not cause mortality or weight loss in the mice, consistent with most human infections. To examine the effect of HCoV-NL63 infection on lung inflammation, lungs were perfused with saline, fixed with formalin, processed for paraffin sectioning, and stained with hematoxvlin and eosin. Lungs from HCoV-NL63-infected hACE2 mice, but not C57BL/6 mice, showed bronchovascular and peribronchial inflammation (Fig. 2, A-C). Three days after inoculation of hACE2 mice, areas of inflammation appeared to correlate with immunofluorescent staining for nsp3 and dsRNA (Fig. 2B). We compared the histological appearance and viral copy number of lungs from NL63-infected mice with lungs from RV-A1B-infected mice (Fig. 2C). There was little or no inflammation 2 days after HCoV-NL63 infection; inflammation peaked 4 days after NL63 infection and was maintained 6 days after infection. In contrast, lung inflammation peaked 2 days after RV-A1B infection and was minimal or absent 6 days after infection. These data are consistent with the time course of viral replication in HCoV-NL63-infected mice (Fig. 1B) and RV-A1B-infected mice, for which vRNA peaked 1 day after inoculation (Fig. 2D). BAL neutrophils and lymphocytes were higher in hACE2 mice compared with wild-type mice (Fig. 3A). There was no significant difference in macrophages or eosinophils between wild-type and hACE2 mice. Lung expression of Ifng, Cxcl1, and Cxcl10 was significantly increased after infection in HCoV-NL63-treated K18hACE2 but not C57BL6/J mice (Fig. 3B). Compared with sham infection, hACE2 mice inoculated with HCoV-NL63 showed airway cholinergic hyperresponsiveness 4 days after inoculation (Fig. 3C). HCoV-NL63-infected hACE2 mice also showed significantly higher airways resistance than HCoV-NL63-infected C57BL/6 mice.

To further characterize the response of hACE2 mice to HCoV-NL63 infection, we analyzed lungs from sham and HCoV-NL63-infected mice using next-generation RNA sequencing. For comparison, we also examined gene expression in RV-A1B-infected mice. In this analysis, the following groups were studied: 1) day 2 after sham infection (LLC-MK2-ACE2 supernatant, n = 3; 2) day 2 after NL63 infection (n = 3); 3) day 4 after HCoV-NL63 infection (n = 3), day 2 after RV-A1B infection (n = 3), and day 4 after RV-A1B infection (n = 3). In this experiment, mean viral copy number two days after infection for the two viruses was comparable (4.85×10^3) copies for NL63 and 4.75×10^3 copies for RV-A1B), despite a 10-fold higher input for RV-A1B. Two days following HCoV-NL63 infection, 433 immune process genes were differentially expressed compared with sham (adjusted P value <0.05), with 189 upregulated and 244 downregulated (volcano plots are shown in Fig. 4A). Of note, numerous IFN-stimulated genes were increased, including Ifi27, Ifi35, Ifi44, Ifih1, Ifit1-3, Ifitm3, Isg15, Isg20, Mx2, Oasl1, and Oasl2. Four days following HCoV-NL63 infection, 707 immune process genes were differentially expressed compared with sham, with 306 upregulated and 401 downregulated. In addition to antiviral genes, genes encoding proinflammatory cytokines were increased including Il1a, Il1b, Il6, Il18, Il33, Nlrp3, Cxcl2, Cxcl3, Ccl6, Ccl9, and Ccl24.

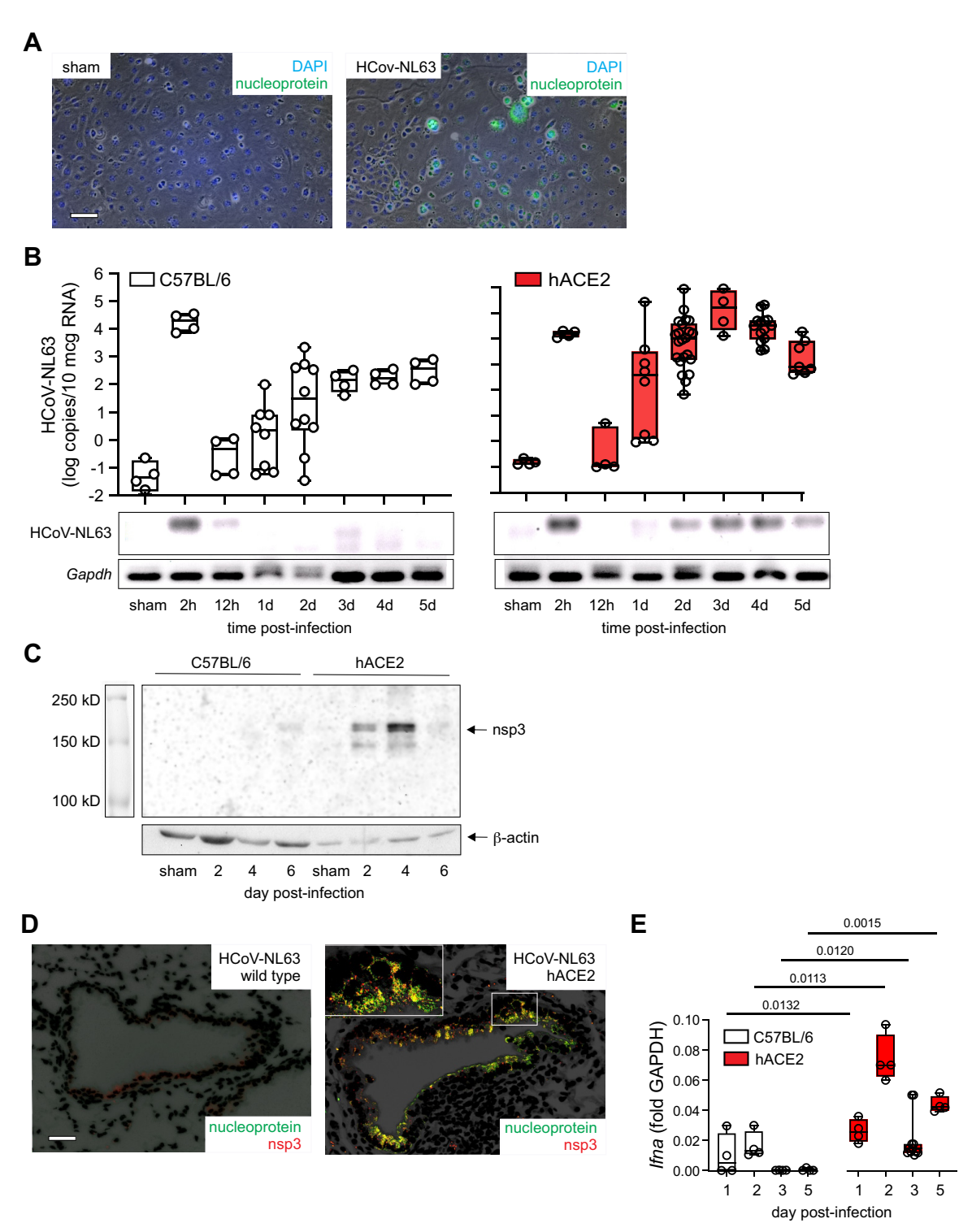


Figure 1. Human coronavirus (HCoV)-NL63 produces a replicative in infection in K18-ACE2 mice. *A*: HCoV-NL63 was titered by examining cytopathic effects in LLC-MK2-ACE2 cells. Cells were infected with sham cell supernatant (*left*) or HCoV-NL63 (*right*). Infection was confirmed by staining with anti-HCoV-NL63 nucleoprotein. The white scale bar is 100 μm. *B*: K18-hACE2 or C57BL6/J mice were inoculated with 50 μL of 1 × 10⁵ TCID₅₀ HCoV-NL63 intranasally and euthanized at 0–5 days posttreatment. Mouse lung viral copy number was assessed by qPCR (total of 7 experiments, n = 4–22) and standard PCR. The amount of "input" virus was measured 2 h after inoculation. C: lung lysates from sham- and HCoV-NL63-infected wild-type and K18-hACE2 mice were immunoblotted for nsp3 and β-actin. *D*: lung sections from wild-type (*left*) and K18-hACE2 mice (*right*) were stained for HCoV-NL63 nucleoprotein (green) and nsp3 (red). The white scale bar is 100 μm. *E*: lung mRNA expression of IFN-α was measured by qPCR (total of 2 experiments, n = 4–8). For all graphs, box and whisker plots show median, 25th and 75th percentiles (hinges of the box), and min and max values (whiskers). Bars indicate results of statistical comparisons between wild-type and hACE2 mice using Kruskal–Wallis test for nonparametric data plus Dunn's multiple comparisons test. ACE2, angiotensin-converting enzyme 2; TCID₅₀, tissue culture infectious dose.

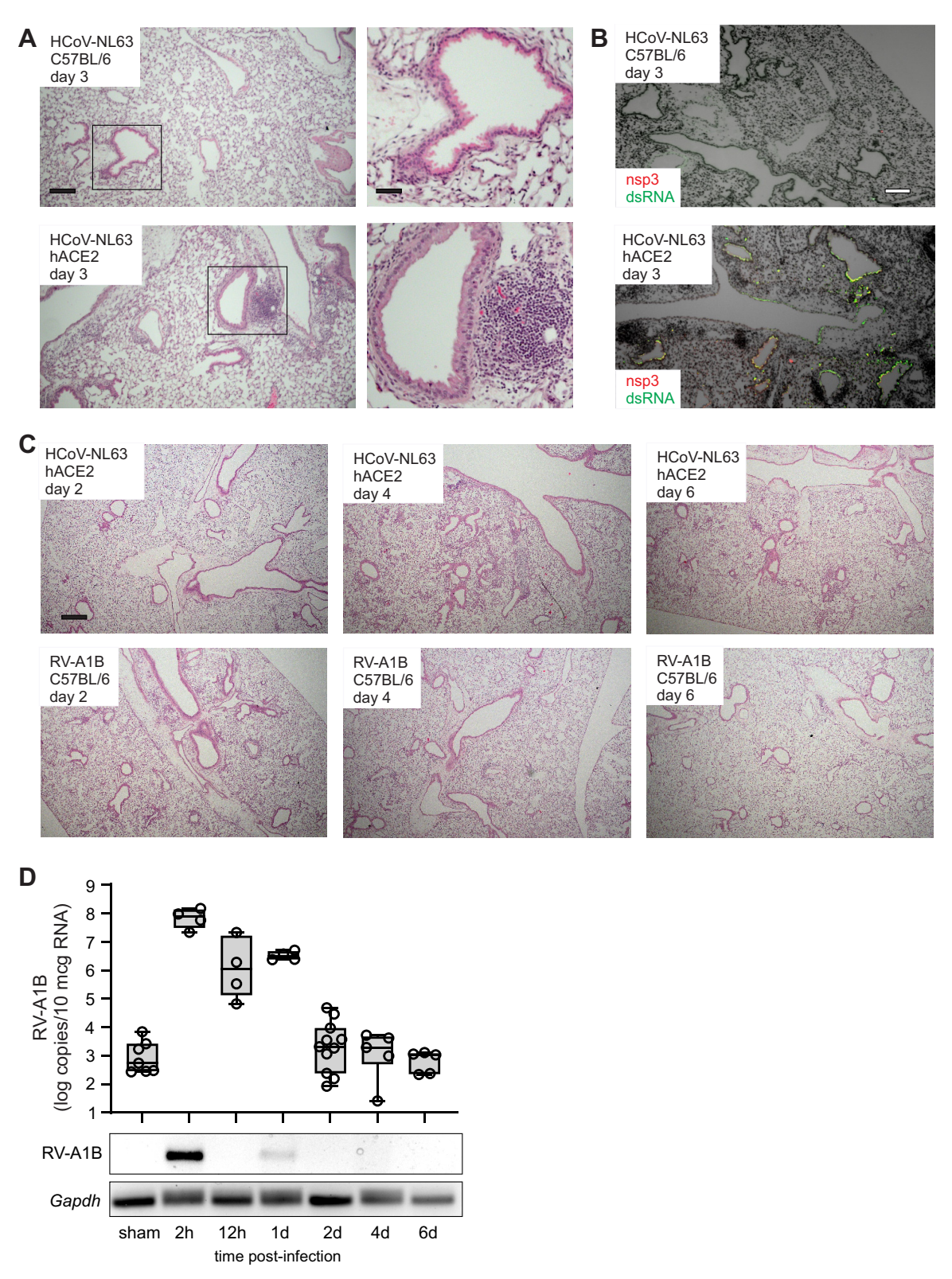
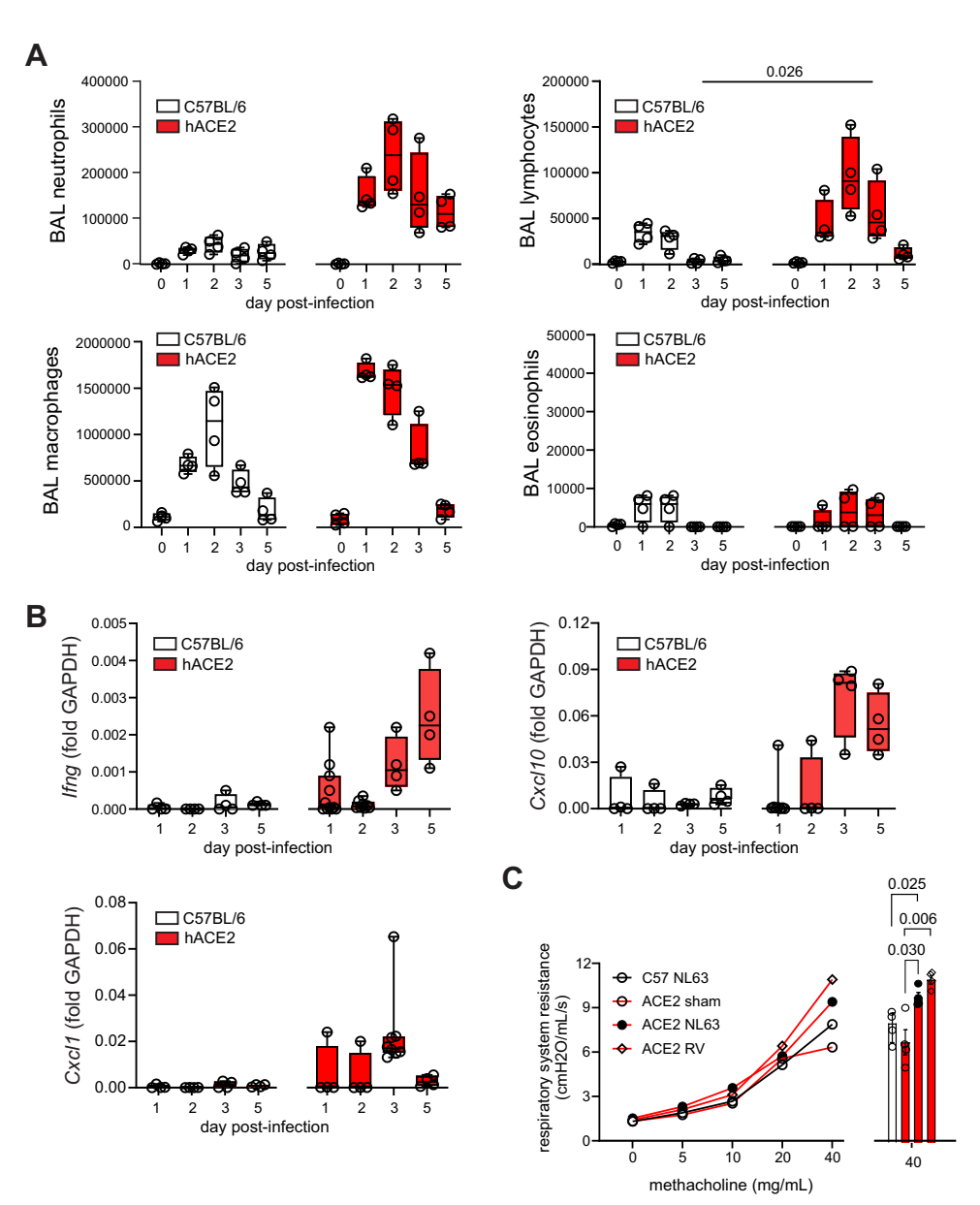


Figure 2. Human coronavirus (HCoV)-NL63 induces lung inflammation in K18-ACE2 mice. K18-hACE2 or C57BL6/J mice were inoculated with HCoV-NL63 intranasally. *A*: lung sections from wild-type (*top*) and K18-hACE2 mice (*bottom*) were stained with hematoxylin and eosin 3 days after infection. In the *left*, the black scale bars are 200 μm. In the *right*,, the black scale bars are 100 μm. *B*: lung sections from wild-type (*top*) and K18-hACE2 mice (*bottom*) were immunostained for nsp3 (red) and dsRNA (green). The white scale bar is 200 μm. C: histological appearance of lungs infected with HCoV-NL63 (*top*) and rhinovirus (RV)-A1B (*bottom*). The black bar is 400 μm. *D*: hACE2 mice were inoculated with 50 μL of RV-A1B intranasally and euthanized at 0-6 days posttreatment. Mouse lung viral copy number was assessed by qPCR and conventional PCR. The amount of "input" virus was measured 2 h after inoculation. Box and whisker plots show median, 25th and 75th percentiles, and min and max values (total of 2 experiments, n = 5–10). ACE2, angiotensin-converting enzyme 2.

Figure 3. Further characterization of HCoV-NL63-infected K18-ACE2 mice. A: bronchoalveolar lavage (BAL) cytospins were stained with hematoxylin and eosin and differential counts determined from 200 cells. BAL neutrophils and lymphocytes were significantly increased in hACE2 mice compared with wild-type mice (results from 2 separate experiments, n = 3 or 4). B: lung mRNA expression was measured by qPCR (total of 2 experiments, n = 4-8). For all graphs, box and whisker plots show median, 25th and 75th percentiles, and min and max values. Bars indicate results of statistical comparisons between wild-type and hACE2 mice using Kruskal-Wallis test for nonparametric data plus Dunn's multiple comparisons test. C: effect of HCoV-NL63 infection on total respiratory system resistance. Methacholine dose-response shows median data for each treatment and concentration; for clarity, individual data and percentiles are not shown. Also shown are individual data points for 40 mg/mL methacholine. Bars indicate results of statistical comparisons two-way ANOVA and Tukey's multiple comparison test.



Two days following RV-A1B infection, 54 genes were differentially expressed compared with sham, with 48 upregulated and 6 downregulated (volcano plots are shown in Fig. 4B). Upregulated genes encoding proinflammatory cytokines included three members of the IL-36 family (Il1f5, Il1f6, and Il1f8) and Cxcl3. Four days following RV-A1B infection, 767 immune process genes were differentially expressed compared with sham, with 356 upregulated and 421 downregulated. In addition to the IL-36 family members, overexpressed cytokines included Il1a, Il6, Il18, Il33, Cxcl2, Cxcl15, Ccl3, Ccl6, Ccl9, Ccl11, and Ccl24. In addition, two interferon response genes were significantly upregulated (Ifi30 and Ifi207).

We also directly compared gene expression patterns between HCoV-NL63 and RV-A1B. On day 2, 728 immune process genes were differentially expressed (adjusted P value < 0.05), with 337 upregulated and 391 downregulated. Compared with RV-A1B, among the immune response genes significantly upregulated by HCoV-NL63 were Ifi27, Ifi35, Isg20, Ifit3, and Cxcl14. In contrast, genes significantly downregulated compared with RV-A1B were proinflammatory, including Il1f5, If1f6, Il1f8, Il1a, Il33, Nlrp3, Cxcl1, Cxcl2, Cxcl3, Cxcl13, Cxcl5, Tlr1, Ccl3, Ccl4, Ccl9, and Ccl24. However, by day 4, there was little difference in the response to the two viruses, with only 129 immune process genes differentially expressed (adjusted P value <0.05), with 33 upregulated and 96 downregulated. Among the immune response genes significantly upregulated by HCoV-NL63 on day 4 compared with RV-A1B were Cxcl3, Il1b, and Nlrp3. Genes significantly downregulated compared with RV-A1B included Il1f5, Il1f6, Cxcl12, and Ccl11.

We examined genes with greater than 1.5-fold changes in expression after viral infection, focusing again on expression of IFNs, antiviral IFN-stimulated proteins, and proinflammatory cytokines and chemokines. On day 2, HCoV-NL63 increased expression of more ISGs and fewer proinflammatory genes as compared with RV-A1B (Fig. 5A). The most

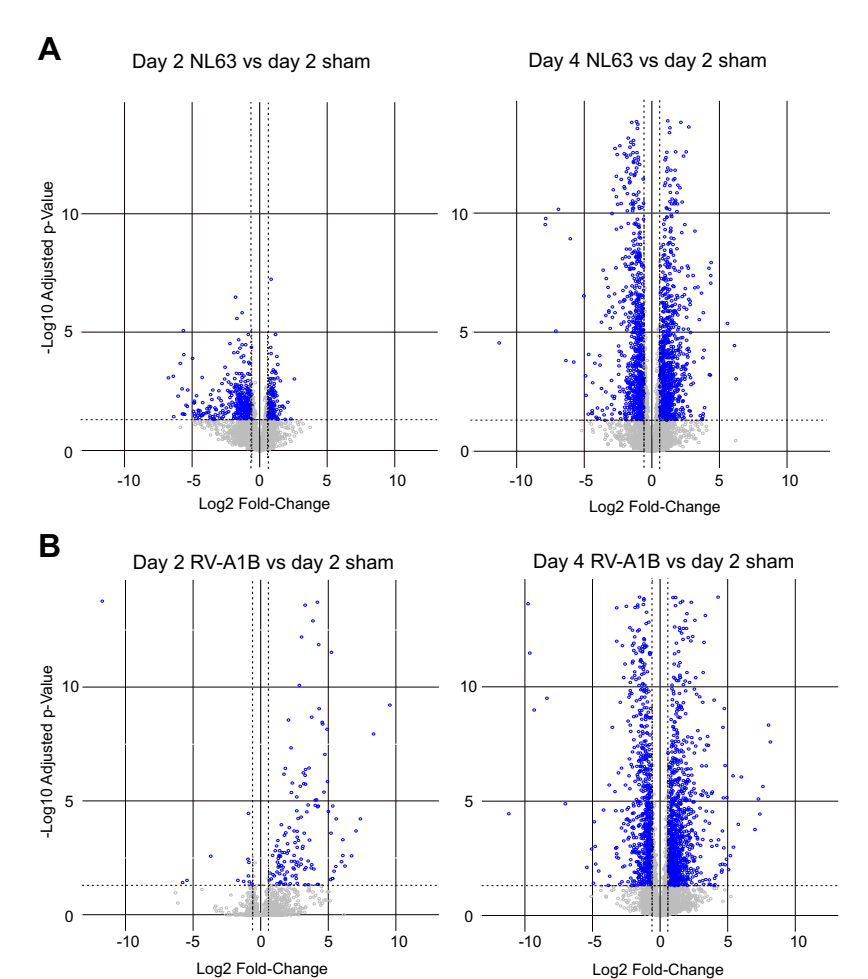


Figure 4. RNA sequencing (RNA-Seq) volcano plots comparing gene expression patterns in response to HCoV-NL63 infection (A) and rhinovirus (RV)-A1B infection (B). A: comparison between HCoV-NL63 infection and sham infection. B: Comparison between RV-A1B infection and sham infection.

highly expressed genes encoded the type I and III IFNs, Ifnb1 and Ifnl3. In contrast, RV-A1B increased expression of more proinflammatory genes and fewer ISGs (Fig. 5B). The most highly expressed genes encoded the IL-36 isoforms, Il1f6 (IL- 36α) and Il1f8 (IL-36 β). By day 4, both infections induced a mix of antiviral and proinflammatory genes. (Complete RNASeq data have been uploaded to NCBI Gene Expression Omnibus under GEO accession number GSE254967; see https://www.ncbi.nlm.nih.gov/geo/query/acc.cgi?acc= GSE254967.)

We then measured transcription of selected genes by qPCR. Compared with sham treatment (LLC-MK2-ACE2 cell supernatant), both HCoV-NL63 and RV-A1B induced mRNA expression of IFNs, IFN-stimulated genes, and proinflammatory cytokines (Fig. 6). There were no statistically significant differences in gene expression between the two viruses except for Ifi35, which was greater after HCoV-NL63. Expression of Mx2 also tended to be higher after HCoV-NL63 infection. Expression of Il1f6, Il1b, Cxcl2, and Cxcl10 tended to be higher after RV-A1B infection.

BAL Cytokines in HCoV-NL63-Infected and RV-A1B-**Infected Mice**

To compare the response to infection in HCoV-NL63infected and RV-A1B-infected mice, we also measured the time course of selected cytokines in the BAL (Fig. 7). HCoV- NL63 significantly increased expression of *Ifna* and *Ifnl*, and RV-A1B significantly increased expression of Ifna, Il1f6, and *IL1b.* Levels of the interferons IFN- α 1 and IFN- λ 2/3 tended to be higher after HCoV-NL63 infection, and levels of the proinflammatory cytokines IL-36α and IL-1β tended to be higher after RV-A1B infection, but there was no statistically significant difference in protein levels between the two viruses.

Infection with RV-A1B Significantly Decreases HCoV-**NL63-Induced Viral Replication and Airway** Inflammation In Vivo

Previous studies revealed that RV-A16 blocks SARS-CoV-2 replication in cultured airway epithelial cells (25) and RV-A1A blocks SARS-CoV-2 replication in airway epithelial organoids (26). We therefore tested whether RV-A1B infection 4 days prior to HCoV-NL63 infection blocks viral replication in our model. Mice were infected with sham or RV-A1B 4 days before HCoV-NL63 infection. Lung RNA was harvested 2 days after sham or HCoV-NL63 infection. Thus, RV-A1B responses were measured 6 days after infection (Fig. 8A). There was no RV-A1B present at this time point (Fig. 2D). Prior RV-A1B infection significantly decreased HCoV-NL63 copy number in hACE2 mice (Fig. 8B). Prior RV-A1B infection also reduced neutrophils and lymphocytes in HCoVinfected hACE2 mice (Fig. 8C) and peribronchial inflammation (Fig. 8D). Finally, prior RV-A1B infection reduced viral

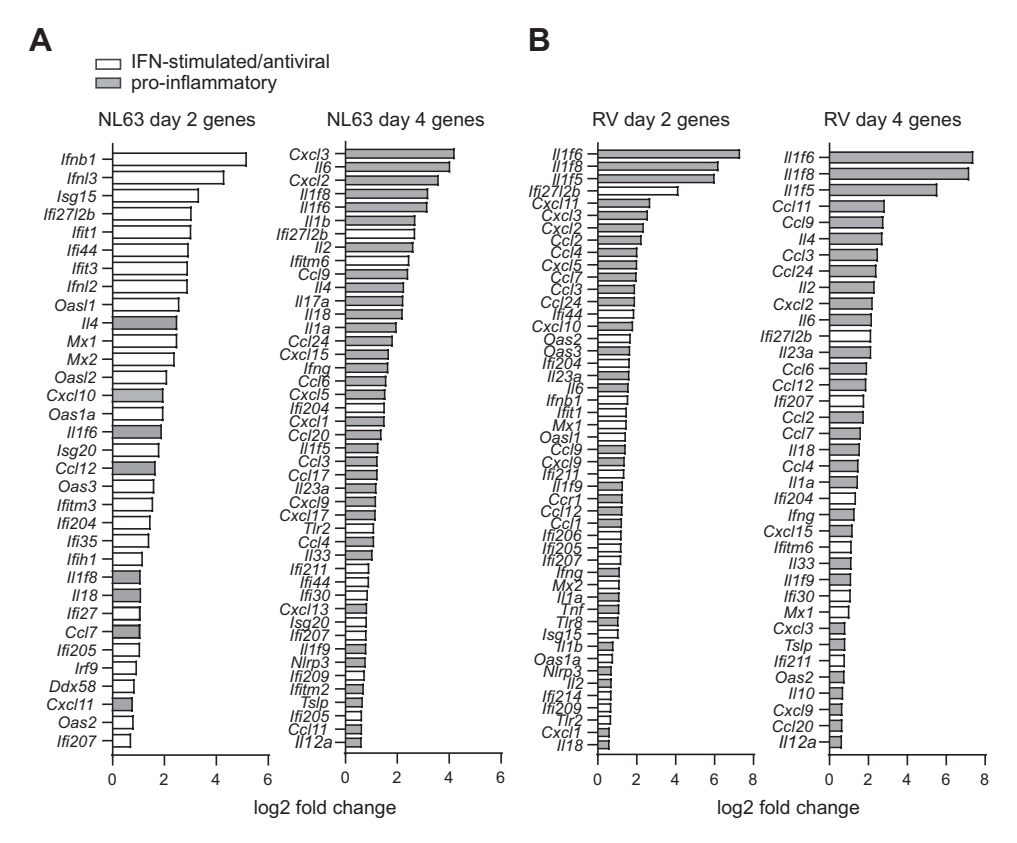


Figure 5. Next-generation RNA sequencing comparing gene expression patterns in response to HCoV-NL63 and rhinovirus (RV)-A1B infection. Immune response genes (including IFN response genes, genes encoding IFNs, antiviral factors, and proinflammatory cytokines) induced by human coronavirus (HCoV)-NL63 (A) and rhinovirus (RV)-A1B infection (B) 2 and 4 days after infection. Data represent mean fold increase vs. sham infection. Genes encoding proinflammatory cytokines are shaded in gray.

expression of nsp-3 (Fig. 8E). There was no effect of RV-A1B infection on hACE2 expression (Fig. 8F).

Effect of Prior RV-A1B Infection on HCoV-NL63-Induced mRNA Expression

Using next-generation RNA sequencing, we compared lungs harvested from ACE2 mice pretreated with RV-A1B 4 days prior to HCoV-NL63 infection (n = 3) with mice that underwent HCoV-NL63 infection (n = 3, described earlier). Lungs were harvested 2 days after HCoV-NL63 infection. Although we found statistically significant differences in gene expression between hCoV-NL63 and sham, RV-A1B and sham, and hCoV-NL63 and RV-A1B (see Fig. 4), there were no statistically significant differences in the expression of immune process genes between RV-A1B + hCoV-NL63 and hCoV-NL63 alone. This was in part because of the small number of samples. Therefore, we examined the immune response genes with the highest fold changes (all of which had log 2 fold change > 0.585 or < -0.585) (Fig. 9). Mice pretreated with RV-A1B showed greater than 1.5-fold reductions in the expression of IFN and IFN-stimulated genes, likely reflecting reduced viral replication. However, when we compared double-infected mice with shamtreated mice, we found that 30 genes were significantly upregulated, including increases in the expression of the antiviral IFN-stimulated genes Mx2, Isg20, and Ifi35. In addition, compared with sham, mice pretreated with RV-A1B showed greater than 1.5-fold increases in many IFN and IFN-stimulated genes including Isg15, Ifi27, Ifi35, Ifi44, Ifi204, Ifi205, Ifi207, Ifi211, Ifit1, Ifit2, Ifit3, Ifih1,

Ifitm3, Irf7, Irf9, Isg20, Mx1, Mx2, Oasl1, Oasla, Oas2, and Oas3 (Fig. 7).

Next, we used qPCR to determine the effect of RV-A1B preinfection on selected genes. We compared four experimental groups: 1) mice inoculated with sham LLC-MK2-ACE2 supernatant 4 days before inoculation with a second dose of sham LLC-MK2-ACE2 supernatant, harvested 2 days after sham infection (sham); 2) mice infected with sham LLC-MK2-ACE2 supernatant 4 days before infection with HCoV-NL63, harvested 2 days after HCoV-NL63 infection (HCoV-NL63); 3) mice infected with RV-A1B 4 days before infection with LLC-MK2-ACE2 cell supernatant, harvested 6 days after RV infection and 2 days after sham infection (RV-A1B); and 4) mice infected with RV-A1B four days before infection with HCoV-NL63, harvested 6 days after RV-A1B infection and 2 days after HCoV-NL63 infection (RV-A1B + HCoV-NL63). Similar to previous results, HCoV-NL63 induced the expression of Ifna, Ifnb1, Ifnl3, and several ISGs including Ifi35, Isg20, Oasl1, and Mx2 (Fig. 10). Increases in IFN and ISG expression were relatively small in response to RV-A1B, likely reflecting the fact that samples were collected 6 days after infection. When we examined HCoV-NL63-induced lung IFN and ISG mRNA expression in mice preinfected with RV-A1B, Ifnb1, Ifnl3, and Ifi35 were significantly decreased compared with HCoV-NL63 alone. None of the IFNs or ISGs were increased by RV-A1B preinfection. However, compared with sham, mice infected with RV-A1B and HCo-NL63 showed increases in Ifi35, Isg20, Oas1, and Mx2 despite the absence of HCoV-NL63 replication, indicating the influence of IFN production by prior RV-A1B infection.

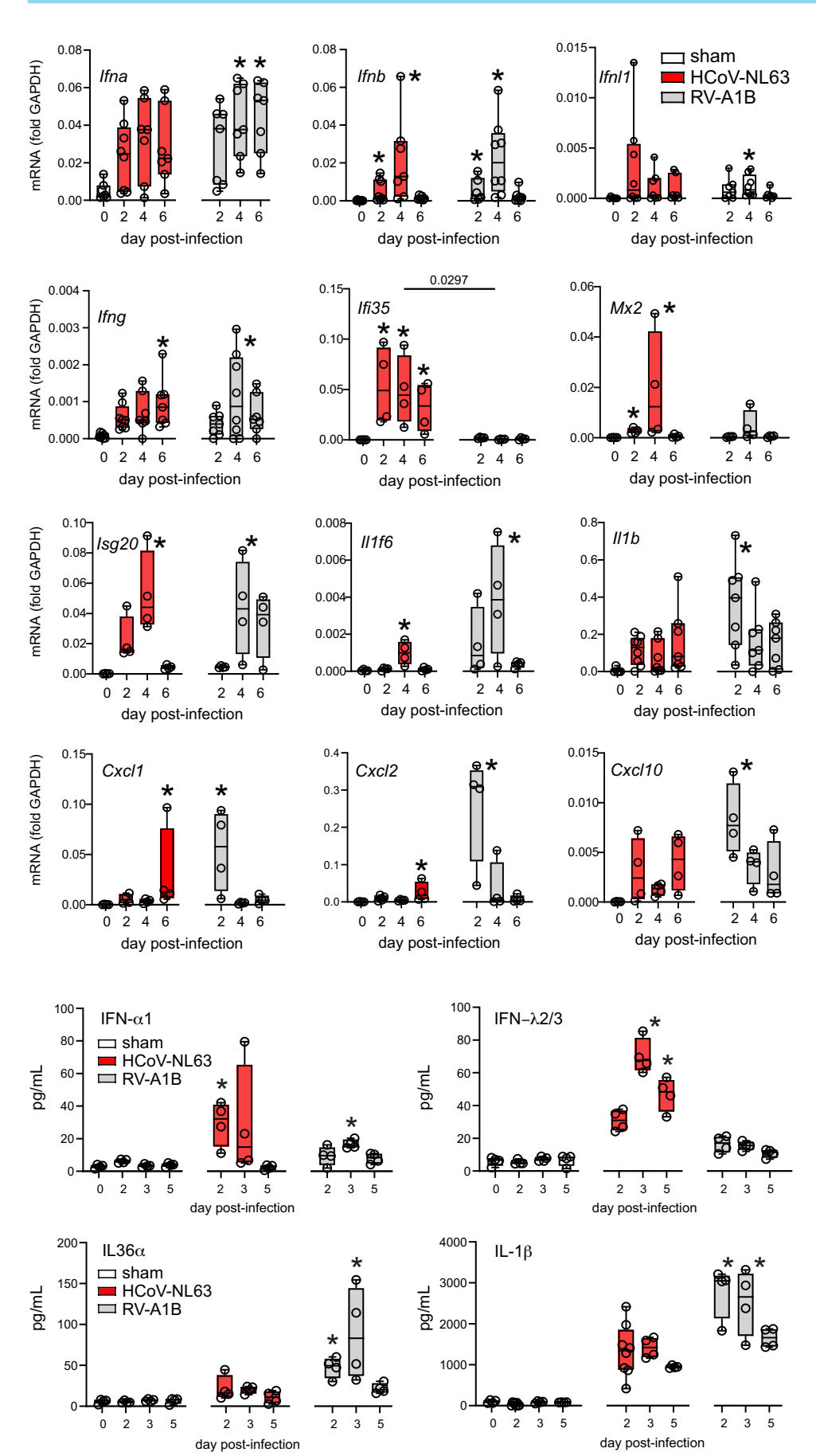
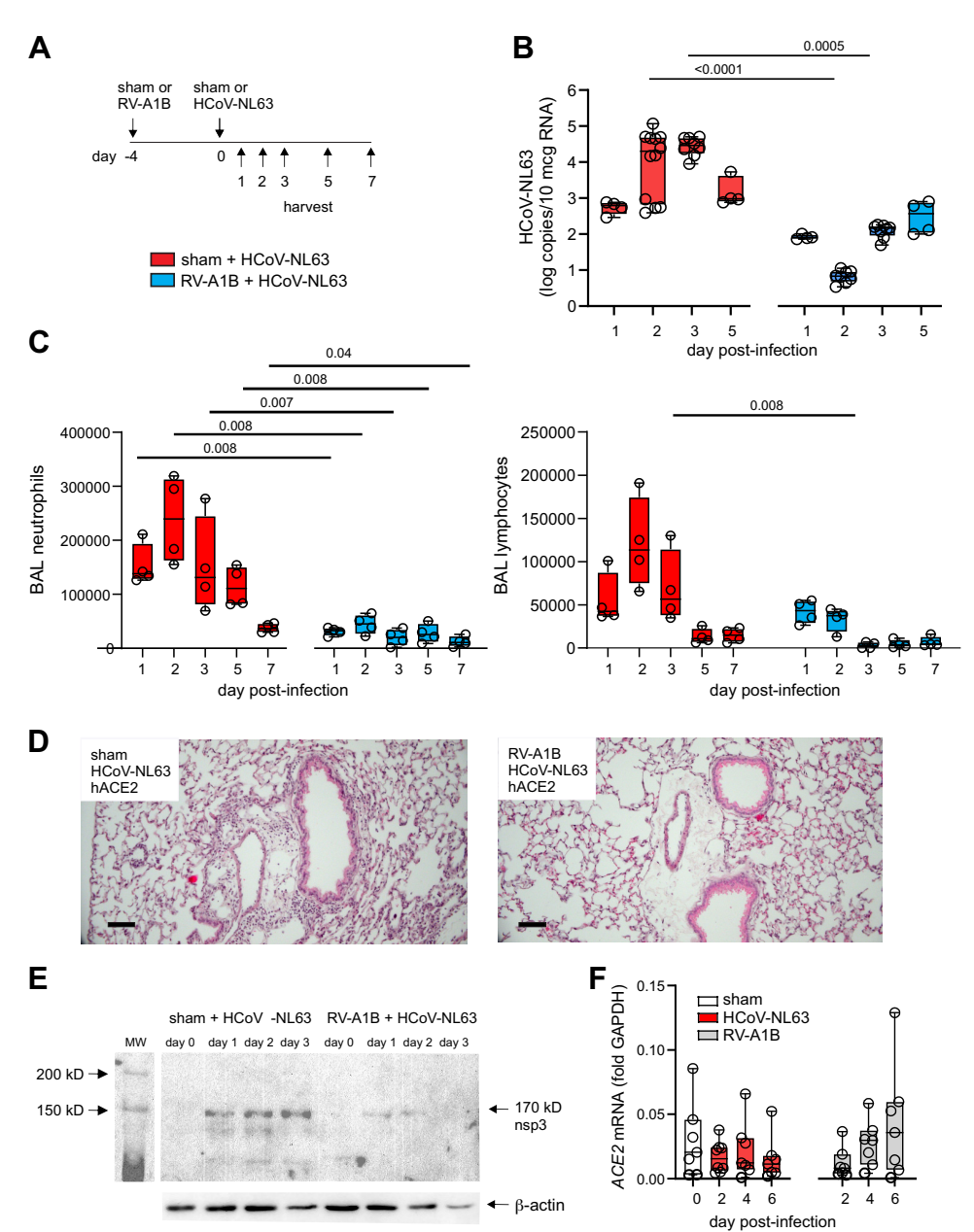


Figure 6. Lung mRNA expression by qPCR in HCoV-NL63- and rhinovirus (RV)-A1B-infected mice. Box and whiskers plots show median, 25th and 75th percentiles, and min and max values. Bars indicate results of statistical comparisons between HCoV-NL63 and RV-A1B. Significant increases vs. sham infection are also shown by the asterisks (*P < 0.05). (One or two experiments each panel, n = 4-8; Kruskal–Wallis test for non-parametric data plus Dunn's multiple comparisons test.)

Figure 7. Bronchoalveolar lavage (BAL) cytokines in human coronavirus (HCoV)-NL63- and rhinovirus (RV)-A1B-infected mice. We measured the time course of selected cytokines in the BAL by ELISA. IL-36 α and IL-1 β tended to be higher after RV-A1B infection, and IFN- α 1 and IFN- λ 2/3 tended to be higher after HCoV-NL63 infection (2 experiments, n = 4-8). Box and whisker plots show median, 25th and 75th percentiles, and min and max values. Bars indicate results of statistical comparisons between HCoV-NL63 and RV-A1B. In addition, significant increases vs. sham infection are also shown by the asterisks (*P < 0.05, Kruskal–Wallis test for nonparametric data plus Dunn's multiple comparisons test).

Figure 8. Rhinovirus (RV)-A1B preinfection attenuates human coronavirus (HCoV)-NL63 replication and airway inflammation in K18-ACE2 mice. A: mice were infected with sham or RV-A1B 4 days before sham or HCoV-NL63 infection. B: lung HCoV-NL63 vRNA was harvested 2 days after HCoV-NL63 infection for viral copy number analysis by qPCR (total of 3 experiments, n = 4-12, the dotted line indicates the detection limit of the assay). C: bronchoalveolar lavage (BAL) cytospins were stained with hematoxylin and eosin and differential counts determined from 200 cells. BAL neutrophils (left) and lymphocytes (right) are shown (results from 2 separate experiments, n = 4/group). D: lung sections from hACE2 mice infected with sham and HCoV-NL63 (left) and hACE2 mice infected with RV-A1B and HCoV-NL63 (right) were stained with hematoxylin and eosin. The black scale bar is 100 μm. E: lung lysates from sham- and HCoV-NL63-infected hACE2 mice (left) and RV-A1B and HCoV-NL63-infected hACE2 mice (right) were immunoblotted for nsp3. F: effect of HCoV-NI 63 and RV-A1B infection on human ACE2 mRNA expression (total of 2 experiments, n = 7). For all graphs, box and whisker plots show median, 25th and 75th percentiles, and min and max values. Bars indicate results of statistical comparisons between HCoV-NL63 and RV-A1B infections using Kruskal-Wallis test for nonparametric data plus Dunn's multiple comparisons test.



RV-A1B infection significantly increased the expression of proinflammatory mRNAs including Il1f6, Tlr2, Il1b, Nlrp3, Ifng, Cxcl10, and Cxcl2 (Fig. 11A). Compared with RV-A1B alone, lungs from mice infected with RV-A1B and HCoV-NL63 showed reduced lung mRNA expression of Il1f6, Nlrp3, Ifng, Cxcl10, and Cxcl2, consistent with the reduced lung inflammation observed in these mice. On the other hand, we identified several transcripts in which RV-A1B preinfection increased HCoV-NL63-induced lung mRNA expression, including Cxcl1 (Fig. 11B). To further examine the effect of RV-A1B preinfection on neutrophil chemoattractants, we examined the protein levels of CXCL1, CXCL2, and CXCL5 by ELISA (Fig. 12). We found that, although HCoV-NL63 alone significantly increased protein abundance of CXCL1, CXCL2, and CXCL5, mice preinfected with RV-A1B did not experience an increase in CXC chemokine expression over sham, consistent with the

reduction in lung neutrophils with double infection. The discrepancy between Cxcl1 mRNA and protein levels of CXCL1 likely represents posttranscriptional regulation.

DISCUSSION

We established a mouse model of HCoV-NL63 using mice expressing human ACE2 under control of the keratin 18 promoter. Compared with wild-type mice, hACE2 mice showed significantly higher levels of HCoV-NL63 vRNA and nsp3, a nonstructural viral protein that is produced in replicating virus. In addition, HCoV-NL63-infected hACE2 mice showed increased BAL neutrophils and lymphocytes, as well as peribronchial and perivascular infiltrates compared with mockinfected controls. Together, these data suggest that HCoV-NL63 causes a replicative infection in hACE2 transgenic

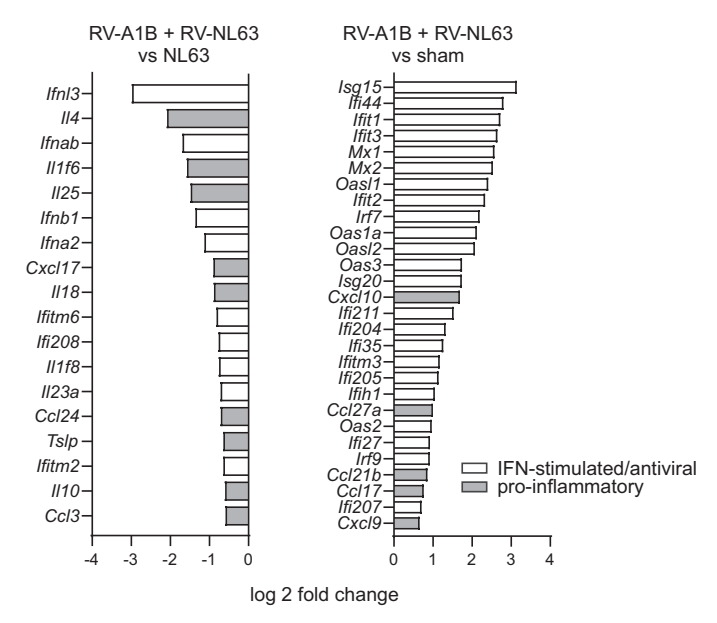


Figure 9. Next-generation RNA sequencing, examining the effect of rhinovirus (RV)-A1B preinfection on gene expression induced by human coronavirus (HCoV)-NL63. Immune response genes (including IFN response genes, genes encoding IFNs, antiviral factors, and proinflammatory cytokines) are shown. Left panel compares RV-A1B + HCoV-NL63 with HCoV-NL63 alone. Right panel compares RV-A1B + HCoV-NL63 with sham infection. Lung samples were taken 2 days after HCoV-NL63 or sham infection. Data represent mean fold increase vs. sham infection. Genes encoding proinflammatory cytokines are shaded in gray.

mice. Our work provides a BSL-2 animal model to study human CoV infection in mice.

Viral infections trigger nearly 80% of asthma exacerbations in children and ~50% in adults (40, 41). An early study showed that HCoVs comprised 17% of all viral infections in children with asthma. We found a similar percentage of HCoV infections in children with asthma (42, 43). Viral infections also induce a substantial fraction of chronic obstructive pulmonary disease exacerbations (44, 45). Understanding of viral-induced exacerbations is incomplete, in part due to the paucity of animal models. We previously developed a mouse model of RV-A1B infection, a minor group virus that binds to LDL-R. Based on partial homology between human and mouse LDL-R, mice infected with RV-A1B show limited viral replication, as evidenced by IFN production and the presence of doublestranded viral RNA (24). However, viral replication is limited and peaks the day after inoculation (24, 46-48). In contrast, HCoV-NL63 replication peaked 3 days after infection of hACE2 mice and persisted for 1 wk. Accordingly, we found that mRNA expression of many IFNs and interferon-stimulated genes was greater for HCoV-NL63 than for RV-A1B, especially on day 2 after infection. qPCR and ELISA data tended to confirm this general chronology. With regard to histological changes, inflammation peaked 4 days after HCoV-NL63 infection and was present 6 days after infection, in contrast with RV-A1B, which peaked 2 days after infection. Thus, by day 4, both viruses induced a proinflammatory gene expression profile. On the other hand, mRNA and protein expression of some proinflammatory genes tended to be higher after RV-A1B infection,

including members of the IL-36 family. Establishment of this mouse model of HCoV-NL63 infection may provide insights into the cellular and molecular mechanisms underlying endemic CoV infections and their potential role in the exacerbation of airway inflammation. In addition, the level of HCoV-NL63 replication in this model might offer advantages compared with RV when studying viral-induced asthma exacerbations. For example, although it has been posited that allergic sensitization interferes with the IFN response to viral infection (49, 50), this cannot easily be tested in the RV model because of limited viral replication and IFN response.

Previous studies have examined the influence of prior RV-A1B exposure on HCoV infection in cultured cells. RV-A16 blocks SARS-CoV-2 replication in cultured airway epithelial cells (25). Cells infected with RV and SARS-CoV-2 showed higher levels of MxA, the product of an interferon-stimulated gene (Mx1) that participates in the cellular antiviral response. As the in vitro efficacy of IFNs against CoVs is well established (51, 52), these data are consistent with the notion that RV-stimulated IFNs block SARS-CoV-2 replication. In addition, it has been shown that RV-A1A blocks SARS-CoV-2 replication in airway epithelial organoids (26). In organoid cultures, SARS-CoV-2 significantly induced ISG expression, but timing was delayed relative to viral replication. Organoids sequentially infected with RV and SARS-CoV-2 showed significantly higher levels of IFN-λ1 production and ISG expression compared with cultures infected with SARS-CoV-2 without prior RV exposure. Using nasal swabs, these investigators also showed that human patients demonstrate a significant enrichment of ISGs after SARS-CoV-2 expression (26). Finally, it has recently been shown that RV protects mice against mouse hepatitis virus strain 1 (MHV-1), a betacoronavirus that naturally infects the enteric tract (53). Mice preinfected with RV had less pulmonary inflammation and hemorrhage and improved survival. However, mice infected with MHV-1 alone had a brisk IFNβ and Mx1 response, and RV infection did not increase Mx1 expression. Administration of a neutralizing antibody against the IFN α/β receptor caused death in mice infected with a nonlethal dose of MHV-1, suggesting that IFNs are required but not sufficient for protection against MHV-1.

In our study, we examined the influence of prior RV-A1B exposure on HCoV-NL63 infection in vivo. We found that prior RV-A1B infection significantly reduced HCoV-NL63 replication and viral-induced peribronchial inflammation, an example of viral interference. However, when we measured IFN and interferon-stimulated gene expression in mice infected with RV-A1B 4 days before HCoV-NL63, there were no instances of increased HCoV-NL63-induced IFN or interferon-stimulated gene mRNA expression after RV-A1B coinfection, including that of Mx1 or Mx2. However, we do not believe that this comparison tells the whole story, as it is possible that IFN and ISG expression was suppressed by the lower viral load in coinfected mice. Indeed, even in the absence of RV-A1B or HCoV-NL63 viral copies, coinfected mice showed higher IFN and ISG mRNA expression, including that of Mx1 and Mx2, than sham-infected mice, as evidenced by both RNA-Seq and qPCR. In addition, although there was no appreciable RV-A1B present 4 days after infection, RV-A1B-induced IFN production persisted until that time. Thus,



Α 0.01 0.02 0.11 0.001 0.002 0.09 0.014 Ifnb1 Ifna 0.012 mRNA (fold GAPDH) 0.010 0.06 sham + sham 0.009 sham + HCoV-NL63 RV-A1B + sham 0.006 0.03 RV-A1B + HCoV-NL63 0.003 0.000 0.00 sham HCoV RV-A1B RV-A1B sham HCoV RV-A1B RV-A1B -NL63 + NL63 -NI 63 + NI 63 В 0.05 0.05 0.008 0.05 0.05 <0.001 0.05 0.002 0.02 <0.001 0.05 0.024 0.04 0.07 GAPDH Ifi35 IfnI3 Isg20 0.05 0.020 mRNA (fold GAPDH 0.03 0.03 0.016 0.015 (fold 0.012 0.02 0.010 mRNA 0.008 0.01 0.005 0.004 0.000 0.00 0.000 HCoV RV-A1B RV-A1B sham HCoV RV-A1B RV-A1B sham HCoV RV-A1B RV-A1B sham -NL63 + NI 63 -NL63 + NL63 -NL63 + NL63 C 0.03 0.003 0.007 0.012 0.012 Mx2 mRNA (fold GAPDH) Oasl1 0.011 0.009 0.010 0.008 0.006 0.006 0.004 0.003 0.002

Figure 10. Effect of prior rhinovirus (RV)-A1B infection on human coronavirus (HCoV)-NL63-induced mRNA expression. A: lung mRNA expression of IFNs and interferon-stimulated genes was measured by qPCR (total of 2 experiments, n = 4-8). Box and whisker plots show median, 25th and 75th percentiles, and min and max values. For A-C, bars indicate results of statistical comparisons using Kruskal-Wallis test for nonparametric data plus Dunn's multiple comparisons test.

in our model, we believe that the preponderance of evidence demonstrates that RV-A1B interferes with HCoV-NL63 infection by enhancing IFN production. We would also like to note that, if RV-A1B attenuates HCoV-NL63 replication by enhancing IFN production, it is conceivable that viral mimetics such as poly I:C (54) or TLR2 agonists (27, 55) could have similar effects on a subsequent viral infection.

0.000

sham HCoV RV-A1B RV-A1E -NL63

+ NL63

In conclusion, we established a mouse model of HCoV-NL63 replicative infection that facilitates studies of the host immune response to endemic human CoV infection. Prior infection with RV-A1B reduced HCoV-NL63 replication and airway inflammation. This model may provide insights into the mechanisms underlying viral-induced asthma exacerbations and viral interference.

DATA AVAILABILITY

Source RNASeg data are openly available at NCBI Gene Expression Omnibus under GEO accession number GSE254967 (see https://www.ncbi.nlm.nih.gov/geo/query/acc.cgi?acc= GSE254967). Additional data are available upon reasonable request.

ACKNOWLEDGMENTS

0.000

We acknowledge support from the Bioinformatics Core of the University of Michigan Medical School's Biomedical Research Core Facilities (RRID:SCR_019168).

sham HCoV RV-A1B RV-A1B

GRANTS

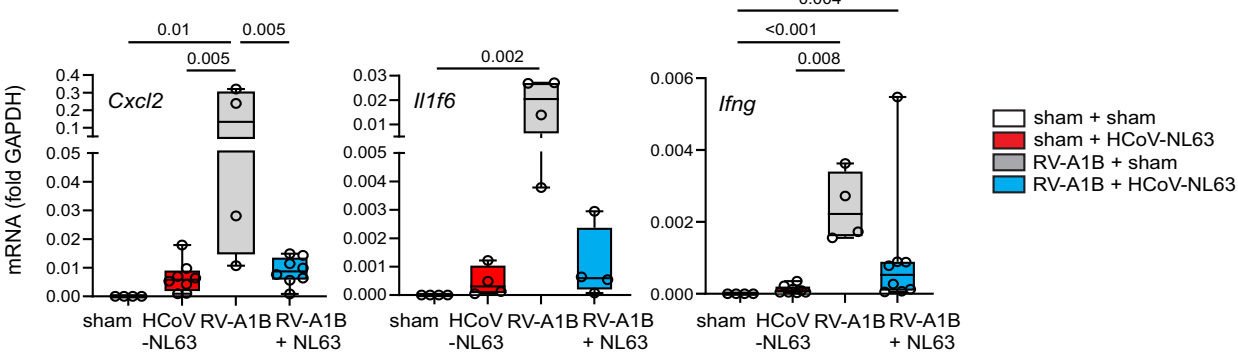
This work was supported by National Institutes of Health Grants Al120526, Al155444 (to M.B.H.), and Al159945 (to S.C.B.) and the Elizabeth Weiser Caswell COVID-19 and Metabolic Disease Grant Program (to M.B.H. and C.N.L.).

DISCLAIMERS

The funders had no role in study design, data collection and analysis, decision to publish, or preparation of the manuscript.

DISCLOSURES

No conflicts of interest, financial or otherwise, are declared by the authors.



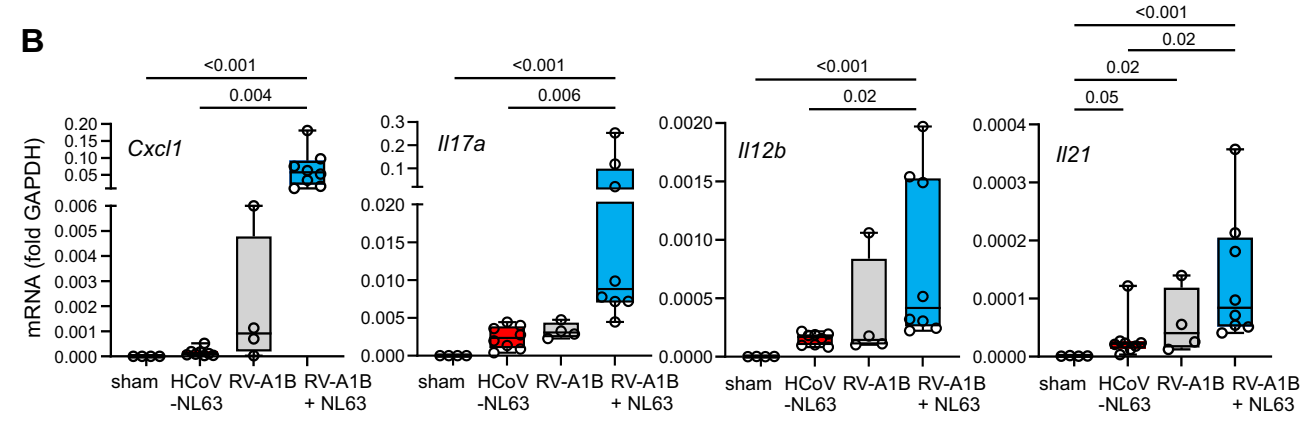


Figure 11. Effect of prior rhinovirus (RV)-A1B infection on human coronavirus (HCoV)-NL63-induced mRNA expression, continued. *A*: lung mRNA expression of selected proinflammatory genes was measured by qPCR. *B*: mRNAs showing an additive for synergistic effect of RV-A1B and HCoV-NL63. Box and whisker plots show median, 25th and 75th percentiles, and min and max values. Total of 2 experiments, n = 4-8, bars indicate results of statistical comparisons using Kruskal–Wallis test for nonparametric data plus Dunn's multiple comparisons test.

AUTHOR CONTRIBUTIONS

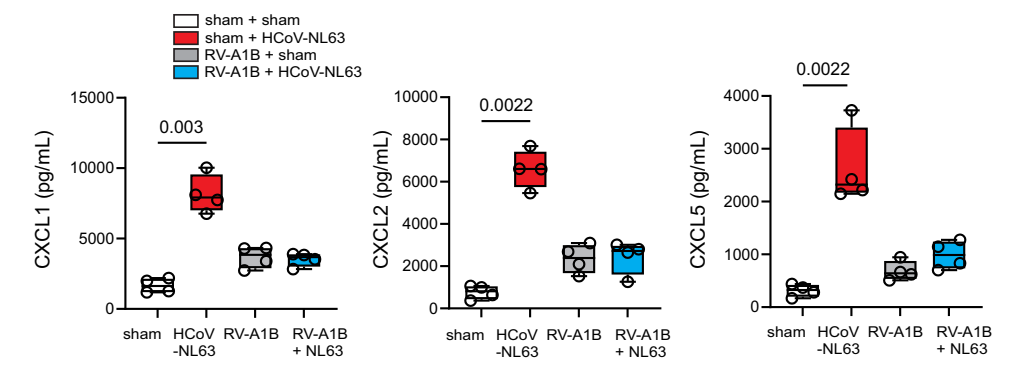
J.K.B., C.N.L., and M.B.H. conceived and designed research; J.K.B., J.E.K., H.A.B., S.S., and J.L. performed experiments; J.K.B., J.E.K., H.A.B., Y.L., and M.B.H. analyzed data; J.K.B. and M.B.H. interpreted results of experiments; J.K.B., J.E.K., H.A.B., and M.B.H. prepared figures; J.K.B. and M.B.H. drafted manuscript; J.K.B., S.C.B., and M.B.H. edited and revised manuscript; J.K.B. and M.B.H. approved final version of manuscript.

REFERENCES

Hamre D, Procknow JJ. A new virus isolated from the human respiratory tract. Proc Soc Exp Biol Med 121: 190–193, 1966. doi:10.3181/00379727-121-30734.

- Tyrrell DA, Bynoe ML. Cultivation of a novel type of common-cold virus in organ cultures. Br Med J 1: 1467–1470, 1965. doi:10.1136/bmj.1.5448.1467.
- McIntosh K, Dees JH, Becker WB, Kapikian AZ, Chanock RM. Recovery in tracheal organ cultures of novel viruses from patients with respiratory disease. Proc Natl Acad Sci USA 57: 933–940, 1967. doi:10.1073/pnas.57.4.933.
- Bradburne AF, Somerset BA. Coronavirus antibody tires in sera of healthy adults and experimentally infected volunteers. *J Hyg (Lond)* 70: 235–244, 1972. doi:10.1017/s0022172400022294.
- van der Hoek L, Pyrc K, Jebbink MF, Vermeulen-Oost W, Berkhout RJ, Wolthers KC, Wertheim-van Dillen PM, Kaandorp J, Spaargaren J, Berkhout B. Identification of a new human coronavirus. Nat Med 10: 368–373, 2004. doi:10.1038/nm1024.
- Woo PC, Lau SK, Chu CM, Chan KH, Tsoi HW, Huang Y, Wong BH, Poon RW, Cai JJ, Luk WK, Poon LL, Wong SS, Guan Y, Peiris JS,

Figure 12. Effect of prior rhinovirus (RV)-A1B infection on human coronavirus (HCoV)-NL63-induced C-X-C chemokine protein abundance measured by ELISA. Box and whisker plots show median, 25th and 75th percentiles, and min and max values (1 experiment, n=4). Bars indicate results of statistical comparisons using Kruskal-Wallis test for nonparametric data plus Dunn's multiple comparisons test.



- Yuen KY. Characterization and complete genome sequence of a novel coronavirus, coronavirus HKU1, from patients with pneumonia. J Virol 79: 884–895, 2005. doi:10.1128/JVI.79.2.884-895.2005.
- Ksiazek TG, Erdman D, Goldsmith CS, Zaki SR, Peret T, Emery S, Tong S, Urbani C, Comer JA, Lim W, Rollin PE, Dowell SF, Ling AE, Humphrey CD, Shieh WJ, Guarner J, Paddock CD, Rota P, Fields B, DeRisi J, Yang JY, Cox N, Hughes JM, LeDuc JW, Bellini WJ, Anderson LJ; SARS Working Group. A novel coronavirus associated with severe acute respiratory syndrome. N Engl J Med 348: 1953-1966, 2003, doi:10.1056/NEJMoa030781,
- Coleman CM, Frieman MB. Emergence of the Middle East respiratory syndrome coronavirus. PLoS Pathog 9: e1003595, 2013. doi:10.1371/journal.ppat.1003595.
- Zhu N, Zhang D, Wang W, Li X, Yang B, Song J, Zhao X, Huang B, Shi W, Lu R, Niu P, Zhan F, Ma X, Wang D, Xu W, Wu G, Gao GF, Tan W; China Novel Coronavirus Investigating and Research Team. A novel coronavirus from patients with pneumonia in China, 2019. N Engl J Med 382: 727-733, 2020. doi:10.1056/NEJMoa2001017.
- Coronaviridae Study Group of the International Committee on Taxonomy of Viruses. The species severe acute respiratory syndrome-related coronavirus: classifying 2019-nCoV and naming it SARS-CoV-2. Nat Microbiol 5: 536-544, 2020. doi:10.1038/s41564-020-0695-7
- Chen Y, Liu Q, Guo D. Emerging coronaviruses: genome structure, replication, and pathogenesis. J Med Virol 92: 418-423, 2020 [Erratum in J Med Virol 92: 2249, 2020]. doi:10.1002/jmv.25681.
- Abdul-Rasool S, Fielding BC. Understanding human coronavirus HCoV-NL63. Open Virol J 4: 76-84, 2010. doi:10.2174/ 1874357901004010076.
- Hofmann H, Pyrc K, van der Hoek L, Geier M, Berkhout B, Pöhlmann S. Human coronavirus NL63 employs the severe acute respiratory syndrome coronavirus receptor for cellular entry. Proc Natl Acad Sci USA 102: 7988-7993, 2005. doi:10.1073/pnas.0409465102.
- Nicholson KG, Kent J, Hammersley V, Cancio E. Acute viral infections of upper respiratory tract in elderly people living in the community: comparative, prospective, population based study of disease burden. BMJ 315: 1060-1064, 1997. doi:10.1136/bmj.315.7115.1060.
- Nicholson KG, Baker DJ, Farquhar A, Hurd D, Kent J, Smith SH. Acute upper respiratory tract viral illness and influenza immunization in homes for the elderly. Epidemiol Infect 105: 609-618, 1990. doi:10.1017/s0950268800048251.
- Falsey AR, McCann RM, Hall WJ, Tanner MA, Criddle MM, Formica MA, Irvine CS, Kolassa JE, Barker WH, Treanor JJ. Acute respiratory tract infection in daycare centers for older persons. J Am Geriatr Soc 43: 30-36, 1995. doi:10.1111/j.1532-5415.1995.tb06238.x.
- Arden KE, Nissen MD, Sloots TP, Mackay IM. New human coronavirus, HCoV-NL63, associated with severe lower respiratory tract disease in Australia. J Med Virol 75: 455-462, 2005. doi:10.1002/ jmv.20288
- McMichael TM, Clark S, Pogosjans S, Kay M, Lewis J, Baer A, Kawakami V, Lukoff MD, Ferro J, Brostrom-Smith C, Riedo FX. Russell D, Hiatt B, Montgomery P, Rao AK, Currie DW, Chow EJ, Tobolowsky F, Bardossy AC, Oakley LP, Jacobs JR, Schwartz NG, Stone N, Reddy SC, Jernigan JA, Honein MA, Clark TA, Duchin JS; Public Health-Seattle & King County, EvergreenHealth, CDC COVID-19 Investigation Team. COVID-19 in a long-term care facility -

- King County, Washington, February 27-March 9, 2020. MMWR Morb Mortal Wkly Rep 69: 339-342, 2020. doi:10.15585/mmwr.mm6912e1.
- Hand J, Rose EB, Salinas A, Lu X, Sakthivel SK, Schneider E, Watson JT. Severe respiratory illness outbreak associated with human coronavirus NL63 in a long-term care facility. Emerg Infect Dis 24: 1964-1966, 2018. doi:10.3201/eid2410.180862
- Verdoni L, Mazza A, Gervasoni A, Martelli L, Ruggeri M, Ciuffreda M, Bonanomi E, D'Antiga L. An outbreak of severe Kawasaki-like disease at the Italian epicentre of the SARS-CoV-2 epidemic: an observational cohort study. Lancet 395: 1771-1778, 2020. doi:10.1016/ S0140-6736(20)31103-X.
- Esper F, Shapiro ED, Weibel C, Ferguson D, Landry ML, Kahn JS. Association between a novel human coronavirus and Kawasaki disease. J Infect Dis 191: 499-502, 2005. doi:10.1086/428291.
- McCray PB Jr, Pewe L, Wohlford-Lenane C, Hickey M, Manzel L, Shi L, Netland J, Jia HP, Halabi C, Sigmund CD, Meyerholz DK, Kirby P. Look DC. Perlman S. Lethal infection of K18-hACE2 mice infected with severe acute respiratory syndrome coronavirus. J Virol 81: 813-821, 2007. doi:10.1128/JVI.02012-06.
- Israelow B, Song E, Mao T, Lu P, Meir A, Liu F, Alfajaro MM, Wei J, Dong H, Homer RJ, Ring A, Wilen CB, Iwasaki A. Mouse model of SARS-CoV-2 reveals inflammatory role of type I interferon signaling. J Exp Med 217: e20201241, 2020. doi:10.1084/jem.20201241.
- Newcomb DC, Sajjan US, Nagarkar DR, Wang Q, Nanua S, Zhou Y, McHenry CL, Hennrick KT, Tsai WC, Bentley JK, Lukacs NW, Johnston SL, Hershenson MB. Human rhinovirus 1B exposure induces phosphatidylinositol 3-kinase-dependent airway inflammation in mice. Am J Respir Crit Care Med 177: 1111-1121, 2008. doi:10.1164/ rccm.200708-1243OC.
- Dee K, Goldfarb DM, Haney J, Amat JAR, Herder V, Stewart M, Szemiel AM, Baquelin M, Murcia PR. Human rhinovirus infection blocks severe acute respiratory syndrome coronavirus 2 replication within the respiratory epithelium: implications for COVID-19 epidemiology. J Infect Dis 224: 31-38, 2021. doi:10.1093/infdis/jiab147.
- Cheemarla NR, Watkins TA, Mihaylova VT, Wang B, Zhao D, Wang G, Landry ML, Foxman EF. Dynamic innate immune response determines susceptibility to SARS-CoV-2 infection and early replication kinetics. J Exp Med 218: e20210583, 2021. doi:10.1084/jem.20210583.
- Bentley JK, Han M, Jaipalli S, Hinde J, Lei J, Ishikawa T, Goldsmith AM, Rajput C, Hershenson MB. Myristoylated rhinovirus VP4 protein activates TLR2-dependent proinflammatory gene expression. Am J Physiol Lung Cell Mol Physiol 317: L57-L70, 2019. doi:10.1152/ aiplung.00365.2018.
- Schildgen O, Jebbink MF, de Vries M, Pyrc K, Dijkman R, Simon A, Müller A, Kupfer B, van der Hoek L. Identification of cell lines permissive for human coronavirus NL63. J Virol Methods 138: 207–210, 2006. doi:10.1016/j.jviromet.2006.07.023.
- Chen Z, Wang Y, Ratia K, Mesecar AD, Wilkinson KD, Baker SC. Proteolytic processing and deubiquitinating activity of papain-like proteases of human coronavirus NL63. J Virol 81: 6007–6018, 2007. doi:10.1128/JVI.02747-06.
- Johnston SL, Tyrrell DAJ. Rhinoviruses. Washington, DC: American Public Health Association, 1997, p. 553-563.
- Papi A, Johnston SL. Rhinovirus infection induces expression of its own receptor intercellular adhesion molecule 1 (ICAM-1) via increased NF-kappaB-mediated transcription. J Biol Chem 274: 9707-9720, 1999. doi:10.1074/jbc.274.14.9707.

- Newcomb DC, Sajjan U, Nanua S, Jia Y, Goldsmith AM, Bentley JK, Hershenson MB. Phosphatidylinositol 3-kinase is required for rhinovirus-induced airway epithelial cell interleukin-8 expression. J Biol Chem 280: 36952-36961, 2005. doi:10.1074/jbc.M502449200.
- Nagarkar DR, Bowman ER, Schneider D, Wang Q, Shim J, Zhao Y, Linn MJ, McHenry CL, Gosangi B, Bentley JK, Tsai WC, Sajjan US, Lukacs NW, Hershenson MB. Rhinovirus infection of allergen-sensitized and -challenged mice induces eotaxin release from functionally polarized macrophages. J Immunol 185: 2525-2535, 2010. doi:10.4049/jimmunol.1000286.
- Dobin A, Davis CA, Schlesinger F, Drenkow J, Zaleski C, Jha S, Batut P, Chaisson M, Gingeras TR. STAR: ultrafast universal RNA-seq aligner. Bioinformatics 29: 15-21, 2013. doi:10.1093/bioinformatics/ bts635.
- Li B, Dewey CN. RSEM: accurate transcript quantification from RNA-35. Seg data with or without a reference genome. BMC Bioinformatics 12: 323, 2011. doi:10.1186/1471-2105-12-323.
- Curran-Everett D, Benos DJ. Guidelines for reporting statistics in journals published by the American Physiological Society: the sequel. Adv Physiol Educ 31: 295-298, 2007. doi:10.1152/advan.00022.2007.
- Love MI, Huber W, Anders S. Moderated estimation of fold change and dispersion for RNA-seq data with DESeq2. Genome Biol 15: 550, 2014. doi:10.1186/s13059-014-0550-8.
- Wu T, Hu E, Xu S, Chen M, Guo P, Dai Z, Feng T, Zhou L, Tang W, Zhan L, Fu X, Liu S, Bo X, Yu G. clusterProfiler 4.0: a universal enrichment tool for interpreting omics data. Innovation (Camb) 2: 100141, 2021. doi:10.1016/j.xinn.2021.100141.
- Lazear HM, Schoggins JW, Diamond MS. Shared and distinct functions of type I and type III interferons. Immunity 50: 907-923, 2019. doi:10.1016/j.immuni.2019.03.025.
- Johnston SL, Pattemore PK, Sanderson G, Smith S, Lampe F, Josephs L, Symington P, O'Toole S, Myint SH, Tyrrell DA, Holgate ST. Community study of role of viral infections in exacerbations of asthma in 9-11 year old children. BMJ 310: 1225-1229, 1995. doi:10.1136/bmj.310.6989.1225.
- Nicholson KG, Kent J, Ireland DC. Respiratory viruses and exacerbations of asthma in adults. BMJ 307: 982-986, 1993. doi:10.1136/ bmj.307.6910.982.
- Lewis TC, Henderson TA, Carpenter A, Ramirez IA, McHenry CL, Goldsmith AM, Ren X, Mentz GB, Mukherjee B, Robins TG, Joiner TA, Mohammad LS, Nguyen ER, Burns MA, Burke DT, Hershenson MB. Nasal cytokine responses to natural colds in asthmatic children. Clin Exp Allergy 42: 1734-1744, 2012. doi:10.1111/cea.12005.
- Lewis TC, Metitiri EE, Mentz GB, Ren X, Goldsmith AM, Eder BN, Wicklund KE, Walsh MP, Comstock AT, Ricci JM, Brennan SR, Washington GL, Owens KB, Mukherjee B, Robins TG, Batterman SA, Hershenson MB; Community Action Against Asthma SteeringCommittee. Impact of community respiratory viral infections in urban children with asthma. Ann Allergy Asthma Immunol 122: 175-183.e2, 2019. doi:10.1016/j.anai.2018.10.021.
- Greenberg SB, Allen M, Wilson J, Atmar RL. Respiratory viral infections in adults with and without chronic obstructive pulmonary disease. Am J Respir Crit Care Med 162: 167-173, 2000. doi:10.1164/ ajrccm.162.1.9911019.

- Seemungal T, Harper-Owen R, Bhowmik A, Moric I, Sanderson G, Message S, Maccallum P, Meade TW, Jeffries DJ, Johnston SL, Wedzicha JA. Respiratory viruses, symptoms, and inflammatory markers in acute exacerbations and stable chronic obstructive pulmonary disease. Am J Respir Crit Care Med 164: 1618-1623, 2001. doi:10.1164/ajrccm.164.9.2105011.
- Wang Q, Miller DJ, Bowman ER, Nagarkar DR, Schneider D, Zhao Y, Linn MJ, Goldsmith AM, Bentley JK, Sajjan US, Hershenson MB. MDA5 and TLR3 initiate pro-inflammatory signaling pathways leading to rhinovirus-induced airways inflammation and hyperresponsiveness. PLoS Pathog 7: e1002070, 2011. doi:10.1371/journal. ppat.1002070.
- Rochlitzer S, Hoymann HG, Müller M, Braun A, U-BIOPRED consortium. No exacerbation but impaired anti-viral mechanisms in a rhinovirus-chronic allergic asthma mouse model. Clin Sci (Lond) 126: 55-65, 2014. doi:10.1042/CS20130174.
- Singanayagam A, Glanville N, Girkin JL, Ching YM, Marcellini A, Porter JD, Toussaint M, Walton RP, Finney LJ, Aniscenko J, Zhu J, Trujillo-Torralbo MB, Calderazzo MA, Grainge C, Loo SL, Veerati PC, Pathinayake PS, Nichol KS, Reid AT, James PL, Solari R, Wark PAB, Knight DA, Moffatt MF, Cookson WO, Edwards MR, Mallia P, Bartlett NW, Johnston SL. Corticosteroid suppression of antiviral immunity increases bacterial loads and mucus production in COPD exacerbations. Nat Commun 9: 2229, 2018. doi:10.1038/s41467-018-04574-1.
- Durrani SR, Montville DJ, Pratt AS, Sahu S, DeVries MK, Rajamanickam V, Gangnon RE, Gill MA, Gern JE, Lemanske RF Jr, Jackson DJ. Innate immune responses to rhinovirus are reduced by the high-affinity IgE receptor in allergic asthmatic children. J Allergy Clin Immunol 130: 489-495, 2012. doi:10.1016/j.jaci.2012.05.023.
- Gill MA, Liu AH, Calatroni A, Krouse RZ, Shao B, Schiltz A, Gern JE, Togias A, Busse WW. Enhanced plasmacytoid dendritic cell antiviral responses after omalizumab. J Allergy Clin Immunol 141: 1735-1743. e9, 2018. doi:10.1016/j.jaci.2017.07.035.
- Schreiber G. The role of type I interferons in the pathogenesis and treatment of COVID-19. Front Immunol 11: 595739, 2020. doi:10.3389/ fimmu 2020 595739.
- King C, Sprent J. Dual nature of type I interferons in SARS-CoV-2-induced inflammation. Trends Immunol 42: 312-322, 2021. doi:10.1016/i.it.2021.02.003.
- Cox G, Gonzalez AJ, Ijezie EC, Rodriguez A, Miller CR, Van Leuven JT, Miura TA. Priming with rhinovirus protects mice against a lethal pulmonary coronavirus infection. Front Immunol 13: 886611, 2022. doi:10.3389/fimmu.2022.886611.
- Mitländer H, Yang Z, Krammer S, Grund JC, Zirlik S, Finotto S. Poly I:C pre-treatment induced the anti-viral interferon response in airway epithelial cells. Viruses 15: 2328, 2023. doi:10.3390/v15122328.
- Girkin J, Loo SL, Esneau C, Maltby S, Mercuri F, Chua B, Reid AT, Veerati PC, Grainge CL, Wark PAB, Knight D, Jackson D, Demaison C, Bartlett NW. TLR2-mediated innate immune priming boosts lung anti-viral immunity. Eur Respir J 58: 2001584, 2021. doi:10.1183/13993003.01584-2020.